IMA Journal of Numerical Analysis (2020) **40**, 976–1004
doi:10.1093/imanum/dry085
Advance Access publication on 27 November 2018

Extending the unified transform: curvilinear polygons and variable coefficient PDEs

MATTHEW J. COLBROOK
Department of Applied Mathematics and Theoretical Physics, University of Cambridge, Cambridge CB3 0WA, UK
m.colbrook@damtp.cam.ac.uk

[Received on 26 June 2017; revised on 23 October 2018]

We provide the first significant extension of the unified transform (also known as the Fokas method) applied to elliptic boundary value problems, namely, we extend the method to curvilinear polygons and partial differential equations (PDEs) with variable coefficients. This is used to solve the generalized Dirichlet-to-Neumann map. The central component of the unified transform is the coupling of certain integral transforms of the given boundary data and of the unknown boundary values. This has become known as the global relation and, in the case of constant coefficient PDEs, simply links the Fourier transforms of the Dirichlet and Neumann boundary values. We extend the global relation to PDEs with variable coefficients and to domains with curved boundaries. Furthermore, we provide a natural choice of global relations for separable PDEs. These generalizations are numerically implemented using a method based on Chebyshev interpolation for efficient and accurate computation of the integral transforms that appear in the global relation. Extensive numerical examples are provided, demonstrating that the method presented in this paper is both accurate and fast, yielding exponential convergence for sufficiently smooth solutions. Furthermore, the method is straightforward to use, involving just the construction of a simple linear system from the integral transforms, and does not require knowledge of Green's functions of the PDE. Details on the implementation are discussed at length.

Keywords: unified transform/Fokas method; elliptic PDEs; boundary value problems; curvilinear polygons; variable coefficients.

1. Introduction

In the late '90s, a new method for analysing boundary value problems (BVPs) for linear and for integrable nonlinear partial differential equations (PDEs) was introduced (Fokas, 1997, 2000, 2001), which has become known as the unified transform, or the Fokas method. Reviews can be found in Fokas (2008), Fokas & Spence (2012), Deconinck *et al.* (2014) and Fokas & Pelloni (2014), with a discussion of the method applied to nonlinear PDEs in Fokas & Sung (2005). The method has been extensively used to numerically (and in some cases, analytically) solve the *generalized Dirichlet-to-Neumann map* for constant coefficient elliptic PDEs formulated in the interior of a polygon (Smitheman *et al.*, 2010; Fornberg & Flyer, 2011; Ashton, 2013; Hashemzadeh *et al.*, 2015). For the Laplace, modified Helmholtz and Helmholtz equations the method expresses the solution in terms of integrals in the complex Fourier plane (Fokas, 2000; Spence & Fokas, 2010a; Davis & Fornberg, 2014). In simple geometries, where the method can be used analytically, it has been used to obtain analytical solutions where classical methods apparently fail (Spence, 2011; Fokas & Kalimeris, 2014) and the method has been put on a rigorous footing by Ashton (Ashton, 2012, 2013). However, the unified transform has thus far only been applied

to PDEs with constant coefficients in polygonal domains.[1] In this paper we provide the first extension of the unified transform to solving the generalized Dirichlet-to-Neumann map on general *curvilinear polygons* and for PDEs with *variable coefficients*. The method proposed in this paper has the following attractive features:

- It is very easy to code up as a numerical method (see Section 4).
- It is fast, with numerical experiments taking at most the order of a few seconds to implement using simple MATLAB code on a standard laptop with 1.80 GHz processor. The time is dominated by setting up the linear system (which requires the computation of certain integrals). As we explain later, this scales linearly with the number of collocation points and is virtually independent of the number of basis functions. It is also trivial to parallelize.
- It is accurate, with convergence rates determined by the expansion basis along the boundary.[2] In particular, spectral convergence is obtained for sufficiently smooth solutions in exactly the same manner as in the case of constant coefficients and polygon domains.
- It is a purely boundary-based method—no discretization of the domain interior is required. However, unlike other boundary methods such as the boundary integral method, it avoids entirely the computation of singular integrals. More importantly, for the setting of variable coefficients we consider here, and in contrast to boundary integral methods, the unified transform *does not require calculation of Green's functions* (these are generally unknown for variable coefficient PDEs except in a few selective cases). It is also very easy to extend the method to obtain the solution at any point in the interior by simply decomposing the domain into smaller subdomains (see Section 5.1).

1.1 *The problem and the unified transform*

The problem of evaluating the generalized Dirichlet-to-Neumann map can be stated as follows. Assume that the PDE is strongly elliptic in the Lipschitz curvilinear polygon Ω, and along each side Γ_j connecting corners z_j and z_{j+1} we are given a relation of the form

$$\delta_j \frac{\partial u_j}{\partial \mathcal{N}} + A_j u_j = g_j, \tag{1.1}$$

where $\delta_j, A_j \in \mathbb{R}$ do not vanish simultaneously and g_j are known functions. In general, the method can also cope with nonconstant, complex valued δ_j, A_j, as well as oblique derivative problems or nonlocal boundary conditions, but for simplicity we consider the above case. Evaluating the generalized Dirichlet-to-Neumann map means solving for the complementary boundary values along Γ_j given by

$$h_j := A_j \frac{\partial u_j}{\partial \mathcal{N}} - \delta_j u_j. \tag{1.2}$$

Recall that for smooth enough given data g_j, there is a unique $H^1(\Omega)$ solution (e.g. McLean, 2000), provided that there is no solution to the homogeneous equation. For certain simple domains and simple

[1] Apart from some simple cases mentioned below.

[2] Our use of a Legendre basis restricts us to algebraic convergence in the presence of corner singularities. Future work will aim at including singular functions in the basis to improve convergence rates in this case.

PDEs, classical methods such as the method of images, separation of variables and eigenfunction expansions can be used to find the associated Green's function and solve this problem explicitly (e.g. Stakgold, 2000). However, in general, this problem must be solved numerically.

Throughout we shall identify $\mathbb{R}^2$ with $\mathbb{C}$ via the complex variable $z = x + iy$. Consider first the simplest case of the two-dimensional Laplace equation formulated in the interior of a closed polygon characterized by the corners $z_j = x_j + iy_j$, $z_j \in \mathbb{C}, j = 1, ..., n$. Define $\hat{u}_j(\lambda)$ as the following Fourier transform along the side (z_j, z_{j+1}):

$$\hat{u}_j(\lambda) = \int_{z_j}^{z_{j+1}} e^{-i\lambda z}\left(\frac{\partial u_j}{\partial \mathcal{N}}\frac{ds}{dz} + \lambda u_j\right)\mathrm{d}z, \quad j = 1, ..., n, \quad \lambda \in \mathbb{C}, \tag{1.3}$$

with $\frac{\partial u_j}{\partial \mathcal{N}}$ denoting the derivative of u in the outward normal to the side (z_j, z_{j+1}) and s denoting the arc length parametrizing this side. The integral transform defined by (1.3) involves both the Dirichlet and Neumann boundary values, however, a well-posed elliptic BVP generally requires prescribing one boundary condition along each part of the boundary. The so called 'global relation' in this case is given by

$$\sum_{j=1}^{n} \hat{u}_j(\lambda) = 0, \quad \lambda \in \mathbb{C}, \tag{1.4}$$

and links the Dirichlet and Neumann boundary values. In some cases the analysis of the global relation implies that the unknown transforms can be computed through the solution of a Riemann–Hilbert problem (Fokas & Kapaev, 2003) and for particular boundary conditions and simple domains this can be bypassed, and the unknown transforms can be computed using only algebraic manipulations. An example is the equilateral triangle for which several results generalizing the classical results of Lamé can be obtained (Dassios & Fokas, 2005; Fokas & Kalimeris, 2014).

In the case of constant coefficient elliptic PDEs on convex Lipschitz domains, it has been shown that the analysis of the global relation actually yields a unique solution (Ashton, 2012) for the unknown boundary values for sufficiently regular boundary data. For the simple case of constant coefficient elliptic PDEs on strict polygons, following the work of several researchers (Fulton *et al.*, 2004; Sifalakis *et al.*, 2007; Sifalakis *et al.*, 2008; Fokas *et al.*, 2009; Sifalakis *et al.*, 2009; Smitheman *et al.*, 2010; Fornberg & Flyer, 2011; Saridakis *et al.*, 2012; Davis & Fornberg, 2014; Hashemzadeh *et al.*, 2015; Ashton 2015a; Colbrook *et al.* (2018)) and in particular the results presented in Fornberg & Flyer (2011), Davis & Fornberg (2014), Hashemzadeh *et al.* (2015) and Colbrook *et al.* (2018), there now exists the following simple algorithm for determining numerically the unknown boundary values of this solution:

(1) Expand $\{g_j\}_1^n$ and $\{h_j\}_1^n$ in terms of $N \in \mathbb{N}$ Legendre polynomials (or some other suitable basis),

$$g_j(t) \approx \sum_{l=0}^{N-1} a_l^j P_l(t), \quad h_j(t) \approx \sum_{l=0}^{N-1} b_l^j P_l(t), \quad j = 1, ..., n, \quad t \in [-1, 1]. \tag{1.5}$$

(2) Express $u_j = (A_j g_j - \delta_j h_j)/(\delta_j^2 + A_j^2)$ and $\partial u_j/\partial \mathcal{N} = (\delta_j g_j + A_j h_j)/(\delta_j^2 + A_j^2)$. Substitute these into the global relation (1.4) to obtain an *approximate global relation* by evaluating at M λ-values in $\mathbb{C}$ (called a collocation set).

(3) Overdetermine the system ($M > nN$) and also evaluate the Schwartz conjugate of the global relation. Solve this system in the least squares sense to determine the vector of the unknown expansion coefficients.

Because this approach involves enforcing the global relations at a set of discrete points in the spectral plane, it is a *spectral collocation method*. This method can be viewed as an alternative to the boundary integral method, where now the key relations are formulated in spectral space rather than physical space. A key advantage of the method, as opposed to many methods which are formulated in the physical space, is that the set of allowed collocation points is very large (typically $\mathbb{C}$ minus a finite set of points). Using this freedom wisely leads to algebraic systems with small condition numbers (Hashemzadeh *et al.*, 2015).

Early numerical implementations of this method used Fourier expansions and were limited to relatively low algebraic rates of convergence (Fulton *et al.*, 2004; Fokas, 2008; Fokas *et al.*, 2009). For sufficiently smooth boundary data, exponential convergence was proven by Ashton and Crooks (Ashton & Crooks, 2016) for a computationally more expensive Galerkin scheme based on the method. Such convergence was realized via the use of Chebyshev rather than Fourier expansions in Sifalakis *et al.* (2008) and Smitheman *et al.* (2010), but, in the case of irregular polygons, the relevant algorithms encountered conditioning and convergence issues. A breakthrough in the numerical implementation of the unified transform was achieved by Fornberg & Flyer (2011); (a) Legendre expansions were introduced and Fourier transforms of the Legendre polynomials were given in terms of Bessel functions. (b) By evaluating the global relation at Halton nodes and by overdetermining the relevant algebraic system, accurate solutions were obtained in an efficient way.

1.2 *Contribution of paper*

Despite the success of the unified transform in solving the above BVP, the major drawback of this method has thus far been its restriction to constant coefficient PDEs and strict polygons (i.e. straight edges). There are three notable exceptions to these limitations: in Fokas (2004) PDEs of the form $u_{xx} + u_{yy} + a(x)u = 0$ were solved on the quarter plane $0 < x, y < \infty$, a separable domain,[3] via the analysis of the global relation, and in Spence & Fokas (2010b,c) integral relations and global relations were constructed for certain domains in polar coordinates, and used to solve BVPs for the Helmholtz equation in a wedge and for the Poisson equation in a circular wedge. However, there has been neither an extension to more general PDEs, or more general domains, nor any numerical implementation of these cases. The final exception to this restriction, related to Spence & Fokas (2010b,c), can be found in Crowdy (2015a,b), which extends the integral transforms of Fokas & Kapaev (2003) to circular regions for the Laplace equation. This was further extended to the biharmonic equation in Crowdy & Luca (2014) and Luca & Crowdy (2018).

In this paper we will show that both of the above drawbacks can be overcome, and extend the unified transform to general *curvilinear polygons* and general *variable coefficient PDEs*. It is found that the use of a Legendre basis still has many advantages in this more general setting. The key observation is that the integral transforms themselves correspond to Legendre coefficients of certain functions. Through the use of a Chebyshev interpolation scheme, Chebyshev coefficients of these functions can be approximated and then converted to the corresponding Legendre coefficients. The advantage of this method is that it is extremely fast (making use of the fast Fourier transform) and very accurate, even for polynomial approximations of large degree. Given this method of computing the integral transforms, we provide

[3] See also Fokas (2004); Treharne & Fokas (2007).

motivation for the proper choice of test functions analogous to the exponential solutions in the case of Laplace equation appearing in (1.3). We provide extensive numerical examples for a variety of elliptic PDEs, including comparisons with the finite element method (FEM), demonstrating that the method, whilst simple, is very robust and accurate.

1.3 *Relation to other methods*

There exists a vast literature on methods seeking to solve above the BVP such as finite element, finite difference, boundary integral methods, spectral methods, etc. It is beyond the scope of this paper to discuss thoroughly the rich literature on PDE methods. However, we feel it appropriate to make a few remarks in this direction.

The closest classical method to the unified transform is the null-field method that originated in the electrical engineering community in the 1960s (e.g. Kleinman *et al.*, 1984). Similarly, to the unified transform, the null-field method is also based on Green's second identity with one of the two functions equal to the solution of the BVP and the other function equal to a family of solutions to the adjoint equation (with no boundary conditions). However, there are significant differences: first, the null-field method is specific to the exterior Helmholtz scattering problem, whereas the unified transform in this paper is applied to interior problems and more general PDEs. Secondly, in the former method one chooses the adjoint solutions to be outgoing wave functions found by separation of variables in polar coordinates, whereas the unified transform has typically chosen the adjoint functions to be the exponential functions found by separation of variables in Cartesian coordinates. Thirdly, in the null-field method one expands the unknown boundary value in a 'global basis', i.e. the basis functions are supported on the whole of the boundary; common choices of the basis are either the outgoing wave functions themselves, or their normal derivatives (see Section 7.7.2 of Martin (2006)). In contrast, the unified transform uses a local basis. Further comparisons with other standard variational methods based on Green's identities can be found in Spence (2014). The unified transform was originally developed using a Lax pair formulation in the theory of integrable nonlinear PDEs, which naturally arises from the differential form of Green's second identity (Fokas & Spence, 2012). In this sense, the unified transform can be viewed as the natural linear limit of inverse scattering transforms used to solve integrable systems.

The unified transform is a boundary-based method, but, in contrast to boundary–integral formulations, it does not involve any singular integrals or Green's functions. Other advantages which are shared with other spectral methods include speed and the fact that one only needs to deal with small-system sizes for suitable basis choices (choices dealing with corner singularities will be discussed elsewhere). There is also a large degree of freedom in how to pick collocation points (typically $\mathbb{C}\backslash\{0\}$). However, unlike many spectral methods (e.g. Boyd, 2001), there is no theory on the optimum choice of collocation points for the unified transform (there is no link with interpolation), with only simple heuristics existing in the literature. Also, in the presence of corner singularities, if one chooses Legendre functions as a basis for expanding the unknown boundary values, one can only achieve algebraic rates of convergence. Adapting the basis to cope with corner singularities was discussed in Colbrook *et al.* (2018) and Fornberg & Flyer (2011), where the unified transform compared well against spectrally accurate boundary integral methods. There are many well-known examples in the literature on how to deal with corner singularities (Li & Lu, 2000), including *hp*-FEM (Guo & Babuška, 1986; Babuška & Guo, 1988; Babuška & Guo, 1989), boundary integral methods (Symm, 1973), Mukhopadhyay *et al.*, 2000), multigrid FEMs (Zhu & Cangellaris, 2006) and collocation methods (such as Trefftz and radial basis methods) (Li *et al.*, 2008; Fornberg & Flyer, 2015). Clearly, adapting the basis used in the unified transform to cope with singularities merits further study.

1.4 *Organization of paper*

The paper is organized as follows. In Section 2 we generalize the global relation to arbitrary divergence form PDEs on curvilinear polygons. The generalized global relation now involves tangential derivatives, as well as the usual Dirichlet and Neumann boundary values that appear in (1.3). Some examples are then given in Section 3. The method and its implementation are extensively analysed in Section 4. Numerical results, including comparisons to finite element and a nonself-adjoint example, are given in Section 5. Finally, we discuss the implications of our results and where they fit into the literature on the unified transform in Section 6.

2. Generalizing the global relation

Suppose that $\alpha(x, y) \in \mathbb{C}^{2\times 2}$ is a matrix valued function, $\beta(x, y) \in \mathbb{C}^2$ a vector valued function and γ a function (all sufficiently smooth) defined over Ω. Consider the formal PDE in divergence form

$$\nabla \cdot (\alpha \nabla u) + \nabla \cdot (\beta u) + \gamma u = 0. \tag{2.1}$$

We assume that the domain Ω is a curvilinear polygon, meaning that it is a bounded connected Lipschitz domain whose boundary consists of a finite number of vertices connected by C^1 arcs. We shall refer to such a domain as a curvilinear polygon and to a standard straight-edged Lipschitz polygon as simply a (strict) polygon. Without loss of generality we shall consider real solutions and real coefficients. We denote the corners of Ω in anticlockwise order as $\{z_j\}_1^n$ with the side Γ_j, joining z_j to z_{j+1} (with the convention that $z_{n+1} = z_1$). Γ_j can be parametrized by

$$[-1, 1] \ni t \to (x_j(t), y_j(t)) \in \mathbb{R}^2,$$

where we assume that the parametrization is C^1 (i.e. the derivative on $(-1, 1)$ can be extended to a continuous function on $[-1, 1]$).

The adjoint of equation (2.1) is given by

$$\nabla \cdot (\alpha^T \nabla v) - \beta \cdot \nabla v + \gamma v = 0. \tag{2.2}$$

We can write the expression $v \times (2.1) - u \times (2.2)$ in the form

$$\nabla \cdot [v(\alpha \nabla u) - u(\alpha^T \nabla v) + \beta uv] = 0. \tag{2.3}$$

Integrating across the domain and applying the divergence theorem we recover the global relation (n denotes the outward normal):

$$\int_{\partial\Omega} u\big[(n \cdot \beta)v - n \cdot (\alpha^T \nabla v)\big] + v\big[n \cdot (\alpha \nabla u)\big]\, \mathrm{d}s = 0. \tag{2.4}$$

Define $l_j(t) = \sqrt{\dot{x}_j(t)^2 + \dot{y}_j(t)^2}$ along the curve Γ_j and assume that $l_j(t) > 0$. Suppose that we have a one-parameter family of solutions of the adjoint equation, $v(x, y; \lambda) = v_\lambda$, for some $\lambda \in \mathscr{C}$, where $\mathscr{C}$

denotes the collocation set. Denoting the solution u along side Γ_j by u_j, the unit outward normal by n_j and analogously the oblique derivative by $n_j \cdot (\alpha \nabla u_j)$, we define the following important transform:

$$\hat{\mu}_j(\lambda) := \int_{-1}^{1} \left\{ u_j \left[(n_j \cdot \beta) v_\lambda - n_j \cdot (\alpha^T \nabla v_\lambda) \right] + v_\lambda \left[n_j \cdot (\alpha \nabla u_j) \right] \right\} l_j(t) \, \mathrm{d}t. \tag{2.5}$$

Using (2.5), the global relation (2.4) becomes

$$\sum_{j=1}^{n} \hat{\mu}_j(\lambda) = 0. \tag{2.6}$$

By choosing α, β and γ appropriately, we can formally treat any PDE of the form

$$a_1(x,y)u_{xx} + a_2(x,y)u_{xy} + a_3(x,y)u_{yy} + b_1(x,y)u_x + b_2(x,y)u_y + c(x,y)u = 0,$$

for sufficiently smooth a_1, a_2, a_3, b_1, b_2 and c. Of course, for a general PDE of the form (2.2), it may be difficult to construct a one-parameter family of solutions.

Remark 2.1 As is usually the case for the unified transform, if u and the PDE coefficients are real-valued and for any λ in our parameter family, there is a corresponding solution of the adjoint equation for $\overline{\lambda}$, then we can obtain a second global relation via Schwartz conjugation, i.e. taking the complex conjugate and replacing λ by $\overline{\lambda}$. This simply replaces $v(x,y;\lambda)$ by $\overline{v(x,y;\overline{\lambda})}$ in the global relation. However, as we shall see in Section 5.2, it is crucial for the numerical implementation of separable equations to consider a complementary global relation obtained via the complementary solution of the ordinary differential equation resulting from separation of variables. For example, in the case of Tricomi, we found it necessary to use both Ai- and Bi-type functions for the y-variable (see Example (3.1)), instead of Ai and the global relation obtained from Ai via Schwartz conjugation.

2.1 *A particular form*

Most examples in this paper will be PDEs of the particular form

$$a(x)u_{yy} + b(y)u_{xx} + cu_{xy} + A(x)u_y + B(y)u_x + d(x,y)u = 0, \quad (x,y) \in \Omega, \tag{2.7}$$

where a, b, A, B, d are given (sufficiently smooth) functions and c is some constant. In the notation of (2.1) this corresponds to

$$\alpha(x,y) = \begin{pmatrix} b(y) & c/2 \\ c/2 & a(x) \end{pmatrix}, \quad \beta(x,y) = \begin{pmatrix} B(y) \\ A(x) \end{pmatrix}, \quad \gamma(x,y) = d(x,y).$$

Suppose that u solves (2.7) and that v solves the corresponding homogeneous adjoint equation:

$$a(x)v_{yy} + b(y)v_{xx} + cv_{xy} - A(x)v_y - B(y)v_x + d(x,y)v = 0, \quad (x,y) \in \Omega. \tag{2.8}$$

We can write the expression $v \times (2.7) - u \times (2.8)$ in the form

$$\frac{\partial}{\partial x}\left[b(y)(vu_x - uv_x) + \frac{c}{2}(vu_y - uv_y) + B(y)uv\right] - \frac{\partial}{\partial y}\left[a(x)(uv_y - vu_y) + \frac{c}{2}(uv_x - vu_x) - A(x)uv\right] = 0. \tag{2.9}$$

We then employ Green's theorem,

$$\iint_{\Omega}\left(\frac{\partial F}{\partial x} - \frac{\partial G}{\partial y}\right)\mathrm{d}x\,\mathrm{d}y = \int_{\partial\Omega}\big(G\mathrm{d}x + F\mathrm{d}y\big), \tag{2.10}$$

to write the global relation (2.4) in the form

$$\begin{aligned}&\int_{\partial\Omega}\left[a(x)(uv_y - vu_y) + \frac{c}{2}(uv_x - vu_x) - A(x)uv\right]\mathrm{d}x\\ &+\int_{\partial\Omega}\left[b(y)(vu_x - uv_x) + \frac{c}{2}(vu_y - uv_y) + B(y)uv\right]\mathrm{d}y = 0.\end{aligned} \tag{2.11}$$

In what follows, $\dot{H}$ will denote the t derivative of the function H and, with an abuse of notation, $\partial H/\partial\mathcal{N}$ will denote the normal derivative of H along the parametrization of the curve Γ_j. With these conventions, it easily follows that $\mathrm{d}x = \dot{x}\,\mathrm{d}t$, $\mathrm{d}y = \dot{y}\,\mathrm{d}t$ and

$$\frac{\partial}{\partial x} = \frac{\dot{x}}{l_j^2}\frac{\partial}{\partial t} + \frac{\dot{y}}{l_j}\frac{\partial}{\partial\mathcal{N}}, \quad \frac{\partial}{\partial y} = \frac{\dot{y}}{l_j^2}\frac{\partial}{\partial t} - \frac{\dot{x}}{l_j}\frac{\partial}{\partial\mathcal{N}}.$$

Thus, the basic transform $\hat{\mu}_j(\lambda)$ becomes

$$\begin{aligned}\hat{\mu}_j(\lambda) = &\int_{-1}^{1}\left\{\left[a(x_j(t))\left(\frac{\dot{y}_j}{l_j^2}\dot{v} - \frac{\dot{x}_j}{l_j}\frac{\partial v}{\partial\mathcal{N}}\right) + \frac{c}{2}\left(\frac{\dot{x}_j}{l_j^2}\dot{v} + \frac{\dot{y}_j}{l_j}\frac{\partial v}{\partial\mathcal{N}}\right) - A(x_j(t))v\right]\dot{x}_j(t)\right.\\ &\left.-\left[b(y_j(t))\left(\frac{\dot{x}_j}{l_j^2}\dot{v} + \frac{\dot{y}_j}{l_j}\frac{\partial v}{\partial\mathcal{N}}\right) + \frac{c}{2}\left(\frac{\dot{y}_j}{l_j^2}\dot{v} - \frac{\dot{x}_j}{l_j}\frac{\partial v}{\partial\mathcal{N}}\right) - B(y_j(t))v\right]\dot{y}_j(t)\right\}u_j\,\mathrm{d}t\\ &+\int_{-1}^{1}\left[\frac{b(y_j(t)) - a(x_j(t))}{l_j^2}\dot{x}_j\dot{y}_j + \frac{c}{2l_j^2}(\dot{y}_j^2 - \dot{x}_j^2)\right]v\dot{u}_j\,\mathrm{d}t\\ &+\int_{-1}^{1}\left[\frac{a(x_j(t))\dot{x}_j^2 + b(y_j(t))\dot{y}_j^2}{l_j} - \frac{c}{l_j}\dot{x}_j\dot{y}_j\right]v\frac{\partial u_j}{\partial\mathcal{N}}\,\mathrm{d}t.\end{aligned} \tag{2.12}$$

This expresses $\hat{\mu}_j(\lambda)$ as an integral transform of the Dirichlet boundary data, as well as the tangential and normal derivatives of u_j that is useful for the boundary conditions given in (1.1).

REMARK 2.2 Note that the global relation now involves the extra information $\dot{u}$ (tangential derivative) as opposed to simply just the Dirichlet and Neumann boundary values when considering the Laplace, modified Helmholtz or Helmholtz equations. This is due to the oblique derivative that appears when applying the divergence theorem.

The global relation simply follows from the fact that the differential form

$$W(x,y;\lambda) = \left[a(uv_y - vu_y) + \frac{c}{2}(uv_x - vu_x) - Auv\right]\mathrm{d}x + \left[b(vu_x - uv_x) + \frac{c}{2}(vu_y - uv_y) + Buv\right]\mathrm{d}y$$

is closed whenever u is a solution of the equation and v a solution of the adjoint equation. Choosing separable exponential solutions to the adjoint equation in the case of the Laplace, the modified Helmholtz or the Helmholtz equations, leads to a simple one form that gives a global relation in terms of the finite Fourier transforms of the relevant boundary values (Hashemzadeh *et al.*, 2015). In these cases we refer the reader to Ashton (2012, 2013) and Ashton & Fokas (2015) for further results.

Another possible route to dealing with curvilinear polygons is to approximate them via strict polygons (this is commonly used in FEMs). However, for accurate approximations this requires polygons whose edges may be very short. Such edges increase the condition number of the linear system in the unified transform (as well as increasing its size) and make the current implementation of the method impractical. Hence, this paper treats curved edges directly since they do not add any more complications other than those that already arise from variable coefficients.

3. Examples of global relations

Given the adjoint equation (2.2), the question of how to construct a one-parameter family of solutions naturally arises. If the PDE is separable then separation of variables allows us to compute a one-parameter family of separable solutions $v(x,y;\lambda)$. Another method is to look for symmetries of the PDE (Hydon, 2000; Oliveri, 2010). Some simple examples are shown below, where we choose λ to avoid branch-cuts/singularities in the domain.

Example 3.1 (Tricomi). Suppose the adjoint equation is

$$v_{yy} + yv_{xx} = 0,$$

i.e. $a(x) = 1$, $b(y) = y$ and $c = A = B = g = 0$ in the notation of Section 2.1. Separation of variables yields the two families of solutions

$$v(x,y;\lambda) = \exp(i\lambda x)\mathrm{Ai}(\sqrt[3]{\lambda^2}y), \quad v(x,y;\lambda) = \exp(i\lambda x)\mathrm{Bi}(\sqrt[3]{\lambda^2}y), \tag{3.1}$$

where Ai and Bi denote the Airy functions of the first and second kind, respectively. Another choice could be given by

$$v(x,y;\lambda) = \left[(x+\lambda)^2 + \frac{4}{9}y^3\right]^{-\frac{1}{6}}. \tag{3.2}$$

This is obtained by considering the particular solution when $\lambda = 0$ and noting that the PDE is invariant under the transformation $x \to x + \lambda$.

Example 3.2 (Generalized Tricomi). Suppose the adjoint equation is

$$v_{yy} + y^{\alpha}v_{xx} = 0,$$

for some $\alpha > 0$. Separation of variables yields the two families of solutions

$$v(x,y;\lambda) = \exp(i\lambda x)\mathrm{Ai}_\alpha(\sqrt[3]{\lambda^2}y), \quad v(x,y;\lambda) = \exp(i\lambda x)\mathrm{Bi}_\alpha(\sqrt[3]{\lambda^2}y), \tag{3.3}$$

where Ai_α and Bi_α denote the generalized Airy functions of the first and second kind, respectively. For $\alpha \neq 1$ we can define these functions in terms of the modified Bessel functions

$$\mathrm{Ai}_\alpha(z) = z^{1/2}K_{1/(\alpha+2)}\Big(\frac{2}{\alpha+2}z^{(\alpha+2)/2}\Big), \tag{3.4}$$

$$\mathrm{Bi}_\alpha(z) = z^{1/2}\Big[I_{1/(\alpha+2)}\Big(\frac{2}{\alpha+2}z^{(\alpha+2)/2}\Big) + I_{-1/(\alpha+2)}\Big(\frac{2}{\alpha+2}z^{(\alpha+2)/2}\Big)\Big]. \tag{3.5}$$

Again, another choice is given by

$$v(x,y;\lambda) = \left[(x+\lambda)^2 + \frac{4}{(\alpha+2)^2}y^{\alpha+2}\right]^{\frac{1}{2}-\frac{\alpha+1}{\alpha+2}}. \tag{3.6}$$

Separation of variables can also be applied to

$$x^\beta v_{yy} + y^\alpha v_{xx} = 0,$$

to yield solutions in terms of products of Ai_α or Bi_α with Ai_β or Bi_β.

EXAMPLE 3.3 (Perturbed Tricomi). Suppose that the adjoint equation is

$$v_{yy} + y(v_{xx} + v) = 0.$$

Separation of variables yields the two families of solutions

$$v(x,y;\lambda) = \exp(i\lambda x)\mathrm{Ai}(\sqrt[3]{\lambda^2-1}y), \quad v(x,y;\lambda) = \exp(i\lambda x)\mathrm{Bi}(\sqrt[3]{\lambda^2-1}y). \tag{3.7}$$

Alternatively, we have solutions of the form

$$v(x,y;\lambda) = \left[(x+\lambda)^2 + \frac{4}{9}y^3\right]^{-\frac{1}{12}}J_{\pm 1/6}\Big(\sqrt{(x+\lambda)^2 + \frac{4}{9}y^3}\Big). \tag{3.8}$$

EXAMPLE 3.4 Suppose that the adjoint equation is

$$v_{yy} \pm \exp(\alpha y)v_{xx} = 0.$$

Separation of variables yields the two families of solutions

$$v(x,y;\lambda) = \exp(i\lambda x)J_0\Big(\frac{2\lambda\exp(\alpha y/2)}{\alpha}\Big), \quad v(x,y;\lambda) = \exp(i\lambda x)Y_0\Big(\frac{2\lambda\exp(\alpha y/2)}{\alpha}\Big), \tag{3.9}$$

for the hyperbolic case and

$$v(x,y;\lambda)=\exp(i\lambda x)I_0\Big(\frac{2\lambda\exp(\alpha y/2)}{\alpha}\Big),\quad v(x,y;\lambda)=\exp(i\lambda x)K_0\Big(\frac{2\lambda\exp(\alpha y/2)}{\alpha}\Big),\tag{3.10}$$

for the elliptic case. Here J_0 and Y_0 denote the Bessel functions of the first and second kind, respectively, whereas I_0 and K_0 denote the modified Bessel functions of the first and second kind, respectively. Another possible choice is

$$v(x,y;\lambda)=\Big[(x+\lambda)^2\pm\frac{4}{\alpha^2}\exp(\alpha y)\Big]^{-\frac{1}{2}}.\tag{3.11}$$

REMARK 3.1 There is a connection between the test functions in (3.1), (3.3), (3.7), (3.10) and the canonical form of the PDE. Namely, under the transformation that maps the elliptic equation to its canonical form, these test functions are analogous to exponential solutions of the adjoint equation. For example, in the case of the Tricomi equation in a domain with $y>0$, the transformation $w=2y^{3/2}/3$ maps the PDE to its canonical form. If $\sqrt[3]{\lambda^2}\notin\mathbb{R}_{\leqslant 0}$ then for large $|\lambda|$ we have (with the $\pm$ depending on branch cuts)

$$\exp(i\lambda x)\mathrm{Ai}(\sqrt[3]{\lambda^2}y)\sim\frac{\exp[\lambda(ix\pm\frac{2}{3}y^{3/2})]}{2\sqrt{\pi}(\sqrt[3]{\lambda^2}y)^{1/4}},$$

whose exponential form is analogous to $\exp(\lambda(ix\pm w))$. Similarly, for the other cases considered in the above examples.

EXAMPLE 3.5 (General Divergence Form Example). Suppose that we take the more general form of (10) with

$$\alpha(x,y)=\begin{pmatrix}(x+\epsilon)^2 & x+\epsilon\\ 0 & 1\end{pmatrix},\quad \beta(x,y)=0,\quad \gamma(x,y)=0.$$

This is elliptic if the domain does not cross the line $x=-\epsilon$. The adjoint is

$$v_{yy}+(x+\epsilon)v_{xy}+(x+\epsilon)^2v_{xx}+2(x+\epsilon)v_x=0$$

and, in particular, the PDE is not formally self-adjoint. We have the family of solutions

$$v(x,y;\lambda)=(x+\epsilon)^{\lambda}\exp\Big(-\frac{\lambda}{2}y\pm\frac{\sqrt{-\lambda(3\lambda+4)}}{2}y\Big).$$

4. The numerical method

We focus on the simplified case of Section 2.1, though the more general case will be discussed in Sections 4.4 and 5.4. There are at least three ingredients necessary for the successful numerical implementation of the method outlined in the introduction:

- A suitable basis choice or equivalently a suitable discretization of boundary values.
- A good choice of test functions $v(x,y;\lambda)$ and of a subset of $\mathscr{C}$ (collocation points) at which to evaluate the global relation.
- Efficient and accurate computation of the integral transforms of the basis functions in the global relation.

4.1 *Basis choice and integral transforms*

The use of Legendre polynomials as a basis choice has had considerable success in the literature since it yields spectral convergence for sufficiently smooth solutions (Fornberg & Flyer, 2011), as opposed to quadratic convergence for a Fourier or sine basis (Fulton *et al.*, 2004; Fokas, 2008; Fokas *et al.*, 2009). It also yields an algebraic system with a much smaller condition number than a Chebyshev basis (Sifalakis *et al.*, 2008; Smitheman *et al.*, 2010). Another key advantage in the strict polygon case for Laplace/Helmholtz-type PDEs is the explicit expression of the finite Fourier transforms of Legendre functions in terms of Bessel functions

$$\hat{P}_l(\lambda) = \int_{-1}^{1} e^{-i\lambda t} P_l(t)\,\mathrm{d}t = \frac{\sqrt{-2\pi i\lambda}}{-i\lambda} I_{l+1/2}(-i\lambda), \quad l = 0, ..., N-1, \quad \lambda \in \mathbb{C}. \tag{4.1}$$

In general, given the definition of $\hat{\mu}_j(\lambda)$ in (2.12), there is no hope of obtaining such an explicit representation for anything, but the most simple arcs Γ_j and functions $v(x, y; \lambda)$. For large $|\lambda|$, if the solution $v(x, y; \lambda)$ has a known asymptotic form, then it would be possible to obtain accurate approximations through the methods of steepest descent/stationary phase. If the integral is oscillatory for large $|\lambda|$, then one could use methods developed in recent years to compute such oscillatory integrals (Olver, 2007; Gamallo *et al.*, 2018). However, it is in fact possible to use the Legendre basis and compute the integral transforms accurately and quickly in a very simple manner. Furthermore, for each side, all of the integral transforms can be computed *simultaneously*. With the approximations in (1.5), the integral transforms are simply linear combinations of rescaled Legendre coefficients of functions, given explicitly in terms of $v, \dot{v}$ and the PDE/side parameters. For example, introducing the functions $F_j(l)$,

$$F_j(l) := \int_{-1}^{1} \Big[\frac{b(y_j(t)) - a(x_j(t))}{l_j^2} \dot{x}_j \dot{y}_j + \frac{c}{2l_j^2}(\dot{y}_j^2 - \dot{x}_j^2) \Big] v P_l(t)\,\mathrm{d}t, \tag{4.2}$$

it follows that $(2l+1)F_j(l)/2$ are simply the Legendre coefficients of the function

$$\Big[\frac{b(y_j(t)) - a(x_j(t))}{l_j^2(t)} \dot{x}_j(t)\dot{y}_j(t) + \frac{c}{2l_j^2(t)}(\dot{y}_j^2(t) - \dot{x}_j^2(t)) \Big] v(x(t), y(t); \lambda), \quad t \in [-1, 1].$$

To compute these, we first compute a high-order Chebyshev interpolation of the integrand and then convert to Legendre coefficients. Given an expansion in terms of M_2 approximated Chebyshev coefficients, stable fast $\mathcal{O}(M_2 \log(M_2)^2)$ methods are available (Hale & Townsend, 2014; Townsend *et al.*, 2018) for the conversion to Legendre coefficients. The interpolation and conversion code are available in the MATLAB package `Chebfun`.[4] This allows us to construct the matrices $\mathscr{D}$, $\mathscr{T}$ and $\mathcal{N} \in \mathbb{C}^{M \times nN}$ corresponding to the integral transforms of the Dirichlet, tangent and

[4] This is freely available at http://www.chebfun.org/. Another option for Julia users is Slevinsky's FastTransforms.jl at https://github.com/MikaelSlevinsky/FastTransforms.jl.

Neumann data, respectively. Explicitly, for collocation points $\lambda_1, ..., \lambda_M$, these transforms are defined as follows:

$$\begin{aligned}\mathscr{D}_{i,(j-1)N+2+l} = \int_{-1}^{1} \Bigg\{ \Bigg[a\Bigg(\frac{\dot{y}_j}{l_j^2}\dot{v}(x_j(t),y_j(t);\lambda_i) - \frac{\dot{x}_j}{l_j}\frac{\partial v}{\partial \mathcal{N}}(x_j(t),y_j(t);\lambda_i)\Bigg) \\ + \frac{c}{2}\Bigg(\frac{\dot{x}_j}{l_j^2}\dot{v}(x_j(t),y_j(t);\lambda_i) + \frac{\dot{y}_j}{l_j}\frac{\partial v}{\partial \mathcal{N}}(x_j(t),y_j(t);\lambda_i)\Bigg) - Av(x_j(t),y_j(t);\lambda_i)\Bigg]\dot{x}_j(t) \\ - \Bigg[b\Bigg(\frac{\dot{x}_j}{l_j^2}\dot{v}(x_j(t),y_j(t);\lambda_i) + \frac{\dot{y}_j}{l_j}\frac{\partial v}{\partial \mathcal{N}}(x_j(t),y_j(t);\lambda_i)\Bigg) \\ + \frac{c}{2}\Bigg(\frac{\dot{y}_j}{l_j^2}\dot{v} - \frac{\dot{x}_j}{l_j}\frac{\partial v}{\partial \mathcal{N}}(x_j(t),y_j(t);\lambda_i)\Bigg) - Bv(x_j(t),y_j(t);\lambda_i)\Bigg]\dot{y}_j(t)\Bigg\} P_l(t)\mathrm{d}t,\end{aligned}$$

$$\mathscr{T}_{i,(j-1)N+2+l} = \int_{-1}^{1}\left(\frac{b-a}{l_j^2}\dot{x}_j\dot{y}_j + \frac{c}{2l_j^2}(\dot{y}_j^2 - \dot{x}_j^2)\right)v(x_j(t),y_j(t);\lambda_i)P_l(t)\,\mathrm{d}t,$$

$$\mathscr{N}_{i,(j-1)N+2+l} = \int_{-1}^{1}\left(\frac{a\dot{x}_j^2 + b\dot{y}_j^2}{l_j} - \frac{c}{l_j}\dot{x}_j\dot{y}_j\right)v(x_j(t),y_j(t);\lambda_i)P_l(t)\,\mathrm{d}t,$$

for $l = 0, 1, ..., N-1$.

We also express the tangential derivatives in terms of our basis expansion by taking the t derivative of the expansion

$$u_j = \frac{A_j g_j - \delta_j h_j}{\delta_j^2 + A_j^2} \approx \frac{1}{\delta_j^2 + A_j^2}\sum_{l=0}^{N-1}(A_j a_l^j - \delta_j b_l^j)P_l(t)$$

and using the well-known Legendre expansions of derivatives of Legendre polynomials. This gives

$$\dot{u}_j \approx \frac{1}{\delta_j^2 + A_j^2}\sum_{l=0}^{N-1}(A_j a_l^j - \delta_j b_l^j)\sum_{m=0, l-m \text{ odd}}^{l-1}(2m+1)P_m(t).$$

To convert the Dirichlet expansion to its tangential counterpart, define the matrix $D \in \mathbb{C}^{N\times N}$ by

$$D_{j-2(k-1)-1,j} = 2(j-2k)+1, \quad j = 1, ..., N, \quad k = 1, ..., \left\lfloor \frac{j+3}{2} \right\rfloor.$$

Now define

$$v_i = \frac{-1}{\delta_j^2 + A_j^2}\sum_{j=1}^{n}\left[A_j(\mathscr{D}_{i,\underline{j}} + \mathscr{T}_{i,\underline{j}}D) + \delta_j\mathcal{N}_{i,\underline{j}}\right]\underline{g}_j, \tag{4.3}$$

where $\underline{g}_j$ denotes the vector $(a_0^j, ..., a_{N-1}^j)^T$ and given a matrix $Q \in \mathbb{C}^{M\times nN}$, $Q_{i,\underline{j}}$ denotes the block portion $\{Q_{i,k}\}_{k=(j-1)N+1}^{jN}$. Finally, define $W \in \mathbb{C}^{M\times nN}$ by

$$W_{i,\underline{j}} = \frac{-\delta_j}{\delta_j^2 + A_j^2}(\mathscr{D}_{i,\underline{j}} + \mathscr{T}_{i,\underline{j}}D) + \frac{A_j}{\delta_j^2 + A_j^2}\mathcal{N}_{i,\underline{j}}, \tag{4.4}$$

where again the subscript j denotes the portion corresponding to the jth side. The linear system we wish to solve can now be expressed (in the case of real-valued solutions) as

$$\begin{bmatrix} W \\ \overline{W} \end{bmatrix} \underline{b} = \begin{bmatrix} v \\ \overline{v} \end{bmatrix}, \tag{4.5}$$

where $\underline{b} = (b_0^1, ..., b_{N-1}^1, b_0^2, ..., b_{N-1}^2, ..., b_0^n, ..., b_{N-1}^n)^T$ is the vector of unknown expansion coefficients and $\bar{\cdot}$ denotes component-wise complex conjugation. For complex solutions we do not include the part with complex conjugation. While scaling of rows does not affect solutions of linear systems with equally many equations as unknowns, it does affect least squares solutions of overdetermined systems. Hence, before proceeding, we normalize to make each row in the coefficient matrix have unit l^1 norm. We then solve this system using MATLAB's backslash command (which uses a QR solver) for a least squares solution approximation of $\underline{b}$.

4.2 *Collocation points*

The final question to consider is the choice of collocation points and test functions. Obviously, this depends on the solutions $v(x, y; \lambda)$ and the resulting set $\mathscr{C}$. For the majority of cases considered in this paper we can choose $\mathscr{C} = \mathbb{C} \backslash \mathscr{S}$, where $\mathscr{S}$ is a simple set consisting of singularities or branch cuts. For convex strict polygons and the Laplace/modified Helmholtz/Helmholtz equations, a suitable choice for collocation points is given in Hashemzadeh *et al.* (2015):

$$\lambda_{j,r} = -(\bar{z}_{j+1} - \bar{z}_j)\frac{R}{2M}r, \quad j = 1, ..., n, \quad r = 1, ..., M, \tag{4.6}$$

where the positive integer M specifies the total number of collocation points (that is given by nM) and the positive number R specifies the distance between consecutive collocation points. In this case the test functions are certain complex exponentials:

$$v(x, y; \lambda) = \exp(-i(\pm x + iy)\lambda), \qquad \text{(Laplace)}, \tag{4.7}$$

$$v(x, y; \lambda) = \exp\left\{i\frac{\kappa}{2}[(\pm x - iy)/\lambda - \lambda(\pm x + iy)]\right\}, \qquad \text{(modified Helmholtz } \nabla^2 - \kappa^2\text{)}, \tag{4.8}$$

$$v(x, y; \lambda) = \exp\left\{-i\frac{\kappa}{2}[(\pm x - iy)/\lambda + \lambda(\pm x + iy)]\right\}, \qquad \text{(Helmholtz } \nabla^2 + \kappa^2\text{)}. \tag{4.9}$$

Such a choice yields an algebraic system with a very small condition number because of the following fact (Fokas *et al.*, 2009) valid for *convex* polygons: for $\lambda = \lambda_{p,r}$ all transforms $\{\hat{\mu}_j(\lambda)\}_1^n$ decay exponentially as $\lambda \to \infty$, except for $\hat{\mu}_p(\lambda)$ that involves an oscillatory integral and for $\hat{\mu}_{p-1}(\lambda)$, $\hat{\mu}_{p+1}(\lambda)$ that decay linearly. This analysis still holds true in the curvilinear case, provided that the polygon is convex. However, lack of convexity can cause serious degrading of the condition number regardless of the collocation choice, though splitting up the polygon can alleviate this problem. Such a splitting is not always possible in the curvilinear case.

In principle, for simple enough PDEs it may be possible to perform a similar analysis as in Fokas *et al.* (2009), leading to curves in the complex plane that yield the same diagonally dominant form of the collocation matrix. However, for the sake of simplicity, we shall evaluate at Halton nodes within a

circle of radius R around the origin. Although these do not lead to as accurate solutions as the above 'ray' choice for Laplace/Helmholtz type PDEs, they are still able to yield extremely accurate results. We leave the investigation of more optimal collocation points to future study.

4.3 *A Simple test*

As a simple test for the method of computing the relevant transforms, we compare the Chebyshev expansion method against explicit evaluation using (4.1). Figure 1 shows the computation of the first 51 Legendre Fourier transforms for $\lambda = 10, 10i, 100, 100i$. As can be seen, the minimum of the absolute and relative errors are negligible. The time taken to evaluate these transforms are shown in Table 1. This suggests that the Chebyshev expansion provides a stable and accurate way to evaluate the more general integral transforms required in the unified transform extremely quickly, and our numerical experiments in Section 5 support this statement.

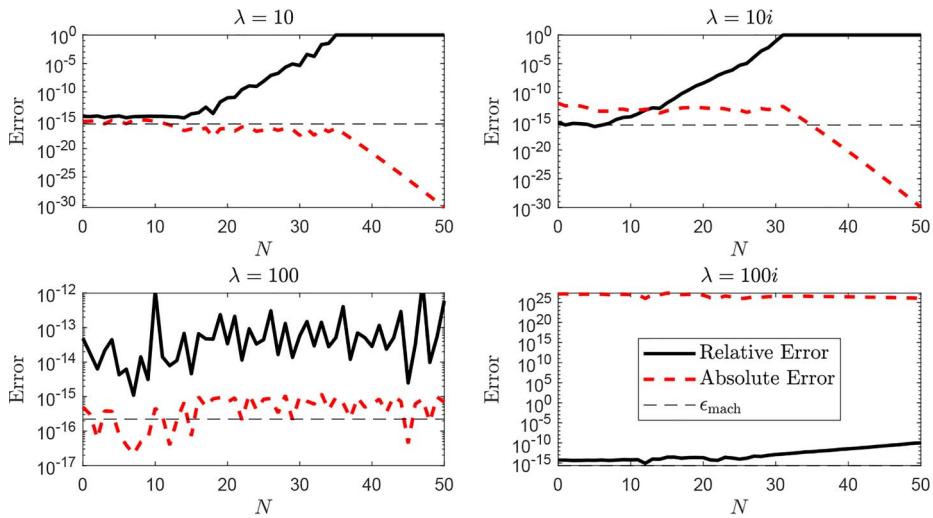

FIG. 1. Absolute and relative errors for computing the Legendre Fourier transforms using the Chebyshev expansions. The linear system setup involves a wide range of different λ and hence, a small absolute or relative error is desirable.

TABLE 1 *Average time taken (seconds) over* 1000 *test runs of computing the first* 51 *Legendre Fourier transforms on a standard laptop with* 1.80 *GHz processor using MATLAB. The Chebyshev method computes all of these simultaneously with negligible difference in times for a larger number of Legendre Fourier transforms. Clearly direct evaluation is quicker, but the Chebyshev method is still very fast and can be applied to the more general integral transforms considered in this paper*

	$\lambda = 10$	$\lambda = 10i$	$\lambda = 100$	$\lambda = 100i$
Proposed method	3.8×10^{-3}	3.7×10^{-3}	5.4×10^{-3}	4.3×10^{-3}
Direct evaluation	2.4×10^{-4}	1.3×10^{-4}	1.3×10^{-3}	1.5×10^{-4}

4.4 *A Natural oblique problem*

Given the divergence form of the PDE, it is easy to apply the method to the following BVP:

$$\hat{\delta}_j n_j \cdot (\alpha \nabla u_j) + \hat{A}_j u_j = g_j \approx \sum_{l=0}^{N-1} a_l^j P_l(t),$$

$$\hat{A}_j n_j \cdot (\alpha \nabla u_j) - \hat{\delta}_j u_j = h_j \approx \sum_{l=0}^{N-1} b_l^j P_l(t),$$

where g_j are known and h_j are unknown. This leads to the following approximate global relation:

$$\sum_{j=1}^{n} \sum_{l=0}^{N-1} b_l^j \int_{-1}^{1} \left\{ \frac{-\hat{\delta}_j}{\hat{\delta}_j^2 + \hat{A}_j^2} [n_j \cdot \beta v_\lambda - n_j \cdot (\alpha^T \nabla v_\lambda)] + \frac{\hat{\delta}_j}{\hat{A}_j^2 + \hat{A}_j^2} v_\lambda \right\} l_j(t) P_l(t)\, \mathrm{d}t$$

$$= - \sum_{j=1}^{n} \sum_{l=0}^{N-1} a_l^j \int_{-1}^{1} \left\{ \frac{\hat{A}_j}{\hat{\delta}_j^2 + \hat{A}_j^2} [n_j \cdot \beta v_\lambda - n_j \cdot (\alpha^T \nabla v_\lambda)] + \frac{\hat{\delta}_j}{\hat{\delta}_j^2 + \hat{A}_j^2} v_\lambda \right\} l_j(t) P_l(t)\, \mathrm{d}t.$$

This can be solved in exactly the same manner as outlined in Section 4.1. Alternatively, assuming the oblique derivative is not tangential, we can solve using the boundary conditions (1.2) by expressing the oblique derivative in terms of the tangential and normal derivatives and employing the methods of Section 4.1. We shall only consider this oblique problem in Section 5.4.

5. Numerical results

We now demonstrate the method on a variety of problems. The numerical implementation is very simple and fast, and only involves the construction of the linear system (4.5). An important benefit of using the proposed method is that in practice the time to set up the matrix scales as $\mathcal{O}(Mn)$, independent of N (although we will allow M to depend on N). Setting up the system is also very easy to parallelize.[5]

5.1 *Laplace, modified Helmholtz and Helmholtz on curved domains*

Our first example considers Laplace- and Helmholtz-type PDEs in a family of curvilinear polygons shown in Fig. 2, parametrized by the position of x_0. These PDEs have been the focus of the literature on the unified transform, but on strict polygons. In particular, we shall study the solution as we vary the position of x_0 and for the choice of adjoint solutions given by (4.8), (4.9) and (4.10), where the $\pm$ takes into account the second global relation obtained via Schwartz conjugation. For the numerical experiments we shall consider the following solutions:

$$u(x, y) = 10 \times \mathrm{Re}\big[J_3(x + iy)\big], \qquad \text{(Laplace)}, \tag{5.1}$$

[5] This was not necessary for the numerical examples in this paper, which can be run in a few seconds when efficiently implemented. However, this parallelization could provide a serious advantage over other methods such as finite elements/finite differences for large M and N.

$$u(x,y) = \exp\left[\frac{\kappa}{\sqrt{2}}(x+y)\right], \qquad \text{(modified Helmholtz)}, \tag{5.2}$$

$$u(x,y) = \cos\left[i\frac{\kappa}{\sqrt{2}}(x+y)\right], \qquad \text{(Helmholtz)}, \tag{5.3}$$

with $\kappa = 2$ for the Helmholtz/modified Helmholtz equations. The parameters used are $x_0 = -3/2$, $R = 30$ (radius of Halton nodes) and $M = 20N$. In general, we found that there was a threshold beyond which increasing M does not effect the accuracy of the solution. The choice of the parameter R is discussed in an appendix. However, the key point to note is that there is a wide range of R that produces very similar results—there is no need for extensive parameter tuning.

We specified mixed data with $(\delta_1, \delta_2, \delta_3, \delta_4) = (1, 1, 0, 1)$ and $(A_1, A_2, A_3, A_4) = (1, 1/2, 1, 0)$. Figure 3 shows the exponential convergence of the computed Legendre coefficients, as well as the condition numbers of the system. The results are qualitatively exactly the same as in the strict polygonal case and were similar for different solutions, A_j, δ_j and κ.

Figure 4 shows the errors of the computed Legendre coefficients and condition numbers of the algebraic system as functions of x_0, for $N = 10$. There is a breakdown in accuracy for x_0 near -2 and 0. The breakdown near 0 occurs due to the domain ceasing to be Lipschitz (cusps develop at $-1 \pm i$) and at this point the condition number of the system increases. These breakdowns can be prevented by

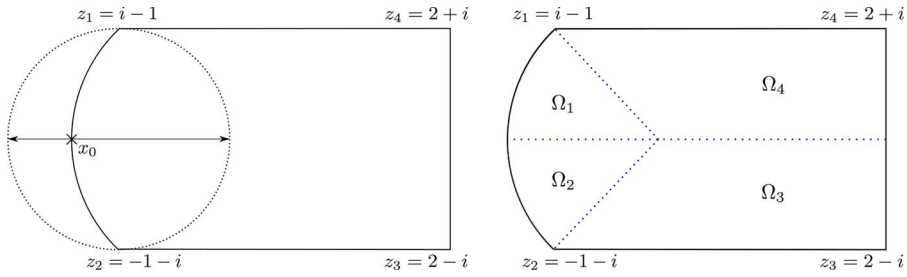

FIG. 2. Domain for the first example, parametrized by the point $x_0 \in [-2, 0]$. The curved side Γ_1 has constant curvature. The subfigure on the right shows the domain decomposition into four subdomains to improve accuracy/conditioning when x_0 is near -2.

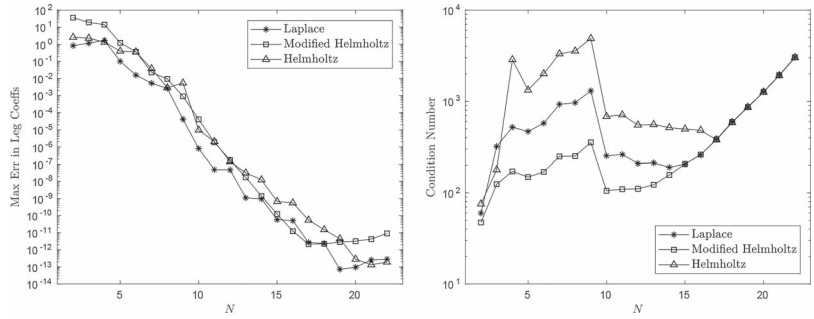

FIG. 3. Left: maximum errors in Legendre coefficients for the unknown boundary values as functions of N. Note the exponential convergence. Right: condition numbers of the systems as functions of N. The parameters for collocation points were *not* optimized (see appendix) and increasing M further reduces the condition number.

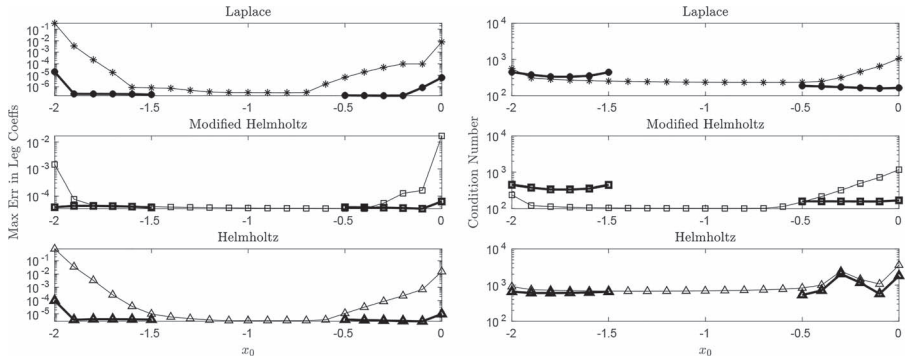

FIG. 4. Left: error as a function of x_0, the bold lines represent errors when we split the domain. Splitting the domain reduces the errors by several orders of magnitude when x_0 is near -2 or 0. Right: analogous plot for the condition numbers.

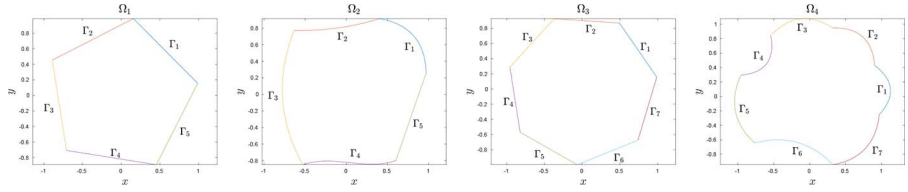

FIG. 5. Curvilinear polygons on which we test the method for the differential operators L_1, L_2 and L_3.

splitting the domain. When x_0 is close to -2, we split into the four domains in Fig. 2 and match the Dirichlet and Neumann data across the artificial edges (i.e. we have four coupled algebraic systems). For points near $x_0 = 0$ we combine Ω_1 and Ω_4, as well as Ω_2 and Ω_3, resulting in two sub-domains. The results are shown in Fig. 4 and further decompositions can reduce the errors further. In general we found it a good strategy to avoid internal angles of π ($x_0 = -2$) or greater. Note also that such a decomposition can be used to find the solution (as well as directional derivatives of the solution) at any point in the interior of the domain.

5.2 *More general elliptic PDEs on curved domains*

In this example, we will consider the three Examples 3.1, 3.3 and 3.4 (elliptic version with $\alpha = 1$) of Section 3 and label the relevant operators as L_1, L_2 and L_3, respectively. For Examples 3.1 and 3.3 we shall shift under a translation of $y \to y + 2$ to ensure ellipticity near the origin. The four domains considered are shown in Fig. 5 and are denoted as Ω_1, Ω_2, Ω_3 and Ω_4. For our test functions we choose the following exact solutions of the relevant adjoint equations:

$$v_1(x,y;\lambda) = \exp(i\lambda x)\mathrm{Ai}[\sqrt[3]{\lambda^2}(y+2)], \qquad v_2(x,y;\lambda) = \exp(i\lambda x)\mathrm{Bi}[\sqrt[3]{\lambda^2}(y+2)], \qquad (L_1),$$

$$v_1(x,y;\lambda) = \exp(i\lambda x)\mathrm{Ai}[\sqrt[3]{\lambda^2-1}(y+2)], \quad v_2(x,y;\lambda) = \exp(i\lambda x)\mathrm{Bi}[\sqrt[3]{\lambda^2-1}(y+2)], \quad (L_2),$$

$$v_1(x,y;\lambda) = \exp(i\lambda x)I_0[2\lambda\exp(y/2)], \qquad v_2(x,y;\lambda) = \exp(i\lambda x)K_0[2\lambda\exp(y/2)]. \qquad (L_3).$$

We set $M = 20N, R = 25$ for L_1 and L_2 and $M = 20N, R = 35$ for L_3. The parameters δ_j and A_j are chosen as follows:

$$(\delta_1, ..., \delta_5) = (1, 0, 1, 1, 0), \qquad (A_1, ..., A_5) = (0, 1, 0, 1, 1), \qquad (\Omega_1 \text{ and } \Omega_2),$$
$$(\delta_1, ..., \delta_8) = (1, 0, 1, 1, 1, 0, 1), \qquad (A_1, ..., A_8) = (0, 1, 0, 1, 1/2, 1, 4), \qquad (\Omega_3 \text{ and } \Omega_4).$$

The analytical solutions we approximate are as follows:

$$u(x, y) = \left[x^2 + \frac{4}{9}(y + 2)^3\right]^{-\frac{1}{6}}, \qquad (L_1),$$
$$u(x, y) = \left[x^2 + \frac{4}{9}(y + 2)^3\right]^{-\frac{1}{12}} J_{1/6}\left(\sqrt{x^2 + \frac{4}{9}(y + 2)^3}\right), \qquad (L_2),$$
$$u(x, y) = \left[x^2 + 4\exp(y)\right]^{-\frac{1}{2}}, \qquad (L_3).$$

The results are shown in Figs 6, 7 and 8. We have labelled three choices of test functions as V_1, V_2 and V_3 corresponding to using only the functions v_1, only the functions v_2, and using both v_1 and v_2 (where we halve M, the number of collocation points, so that the matrix sizes are the same across our experiments), respectively. There are a few observations that are worth mentioning:

- In each case we observe exponential convergence for V_3 due to the smoothness of the analytical solutions.
- The errors are smaller for the more regular polygons (Ω_1 and Ω_3) than the irregular curved polygons.
- For the Tricomi type operators (L_1 and L_2), the errors are much smaller when we use both types of test functions (V_3) as opposed to only one type.

These results demonstrate that it is straightforward to implement the unified transform in curvilinear polygons and for elliptic PDEs with variable coefficients.

5.3 *Generalized Tricomi*

In this example we will consider the generalized Tricomi equation

$$(x + 2)u_{yy} + (y + 2)^2 u_{yy} = 0,$$

for the two domains shown in Fig. 9. We set $R = 5$ for Ω_1 and $R = 10$ for Ω_2, with $M = 20N$ for both domains. Based on the evidence in Section 5.2, we evaluated the global relations with the two types of test functions given by

$$v(x, y; \lambda) = \left\{ \begin{array}{c} \mathrm{Ai}[\lambda(x + 2)] \\ \mathrm{Bi}[\lambda(x + 2)] \end{array} \right\} \cdot \mathrm{Ai}_2[\lambda^{3/4} e^{i\pi/4}(y + 2)].$$

We have found that this considerably outperformed the choice of using only one type of separable solution as a test function (however, the results were not improved upon using Bi_2 type solutions in the y variable as well).

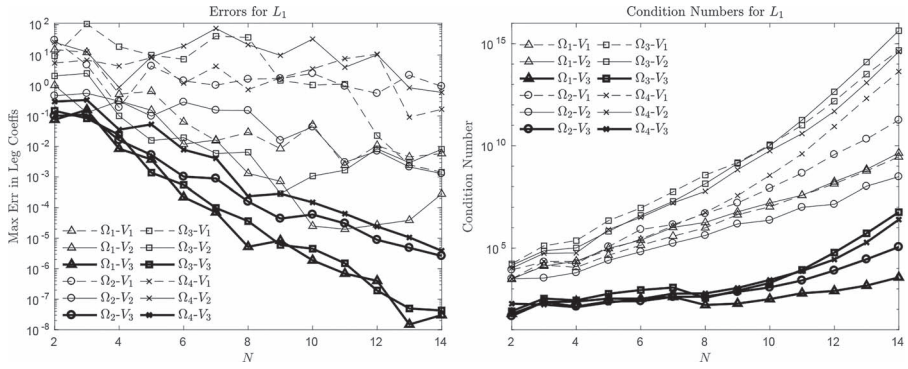

FIG. 6. Maximum errors in computed Legendre coefficients and condition numbers for the operator L_1.

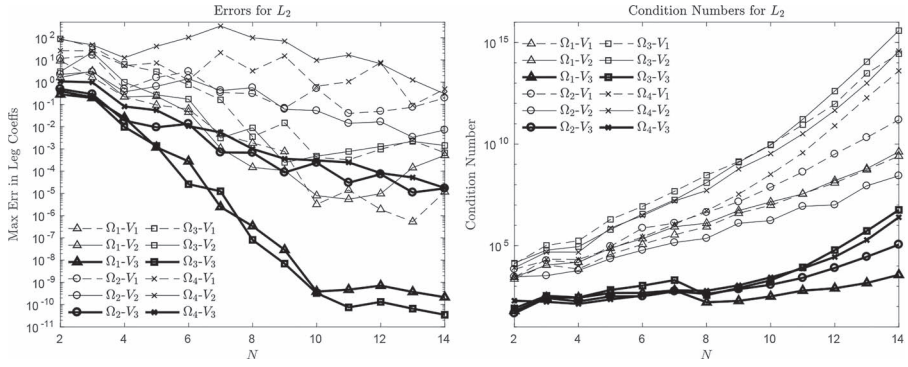

FIG. 7. Same as Figure 6, but for L_2.

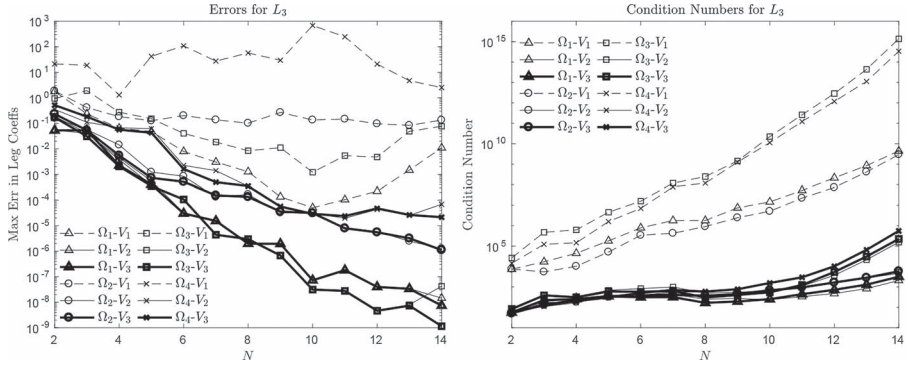

FIG. 8. Same as Figure 6, but for L_3.

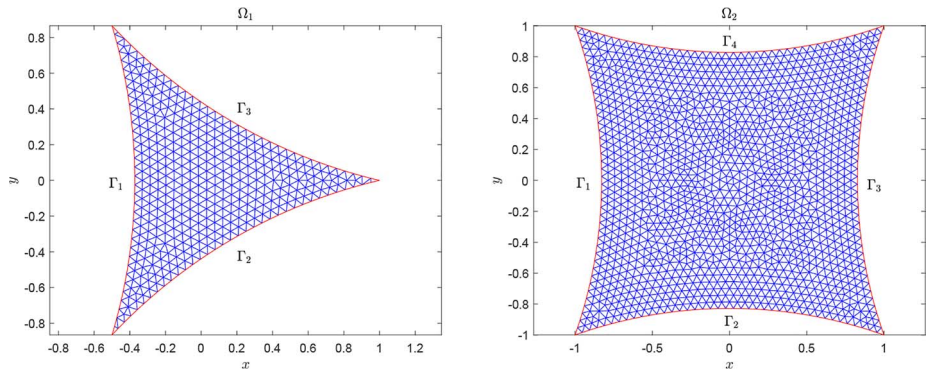

FIG. 9. Domains for which we treat the generalized Tricomi equation. We have also shown an example triangulation for our comparisons with FEM (the triangulation used was much finer).

Our first test uses the following parameter choices:

$$(\delta_1,\delta_2,\delta_3)=(1,0,1), \qquad (A_1,A_2,A_3)=(1/2,1,0), \qquad (\Omega_1),$$
$$(\delta_1,\delta_2,\delta_3,\delta_4)=(1,0,1,1), \qquad (A_1,A_2,A_3,A_4)=(1/2,1,0,1), \qquad (\Omega_2)$$

and the analytic solution

$$u(x,y)=\mathrm{Ai}(x+2)\mathrm{Re}\{\mathrm{Ai}_2[e^{i\pi/4}(y+2)]\}.$$

As before, the method converges exponentially to this solution with the results for $N=16$ (Ω_1) and $N=22$ (Ω_2) shown in Fig. 10.

Finally, we consider a case where the solution is not known analytically. We set $A_j=1$ and $\delta_j=0$, a Dirichlet problem, with

$$u(x,y)=\sin(x), \quad (x,y)\in\partial\Omega.$$

Such a boundary condition will cause corner singularities in the solution and hence, we only expect algebraic convergence. The algebraic convergence is shown in Fig. 11, where we plot the maximum error over the points $t=-0.99,-0.98,...,0.99$, along each side against N. The error is estimated by comparing to larger N and also to the solution calculated using the FEM. The convergence for FEM (linear and quadratic elements) is shown in Fig. 13. The difference in the number of degrees of freedom ($nN\approx 100$ for the unified transform) needed to gain a given error tolerance is striking. Of course, the algebraic rate of convergence of the unified transform with the Legendre basis will struggle to compete with methods such as adaptive h-FEM[6] or exponential convergence of special boundary integral methods (the latter also offers the advantage of boundary-based methods, namely much fewer degrees of freedom needed). However, the unified transform has a significant pedagogical advantage: the numerical implementation of the method is straightforward so that even undergraduate students can implement it using MATLAB. Future work will aim at dealing with corner singularities in the context of the unified transform to improve the rate of convergence. Another important point is reflected by

[6] Or hp-FEM, but it should be noted that such schemes which take $p\to\infty$ generally have very high complexity with the notable exception of Beuchler & Schoeberl (2006) so that it is common to restrict to polynomial orders <10.

our choice of comparisons with FEM (rather than say boundary integral methods). Although boundary integral methods require much fewer degrees of freedom than FEM to compute the unknown boundary values, they require the calculation/integration of Green's functions. For variable coefficient PDEs, the Green's functions are largely unknown or, if they are known, they are complicated. Hence, a key advantage of the unified transform is that it provides a boundary method that does not need knowledge of the corresponding Green's function.

5.4 *An oblique derivative problem*

In this final example we shall test the method for the PDE given by Example 3.5 using the test functions

$$v(x, y; \lambda) = (x + \epsilon)^{\lambda} \exp\Big(-\frac{\lambda}{2} y \pm \frac{\sqrt{-\lambda(3\lambda + 4)}}{2} y \Big).$$

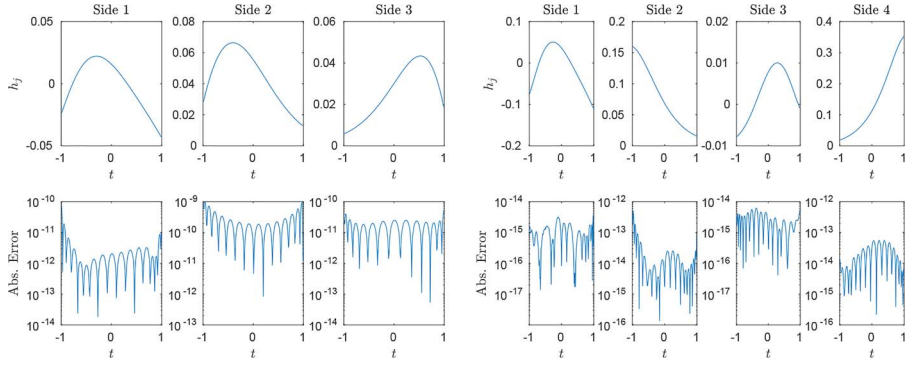

FIG. 10. Results for problem with analytically known solution. Left: $N = 16$ and Ω_1. Right: $N = 22$ and Ω_2.

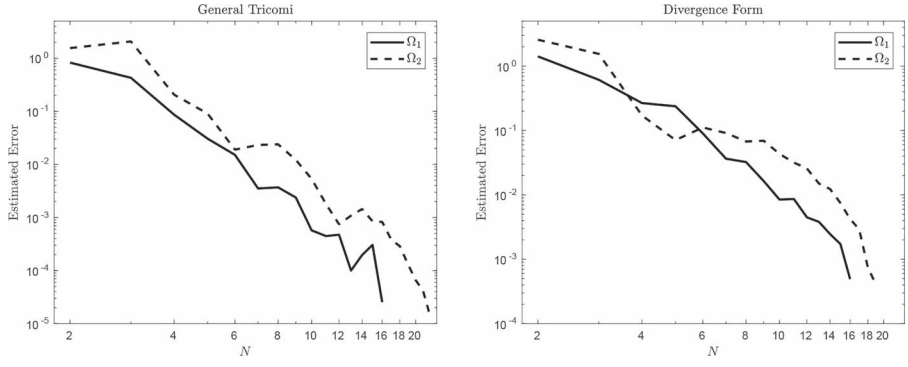

FIG. 11. Convergence rates in presence of corner singularities for the unified transform. Left: algebraic convergence for Dirichlet problem for the generalized Tricomi equation. Right: algebraic convergence for Dirichlet problem for the general divergence problem.

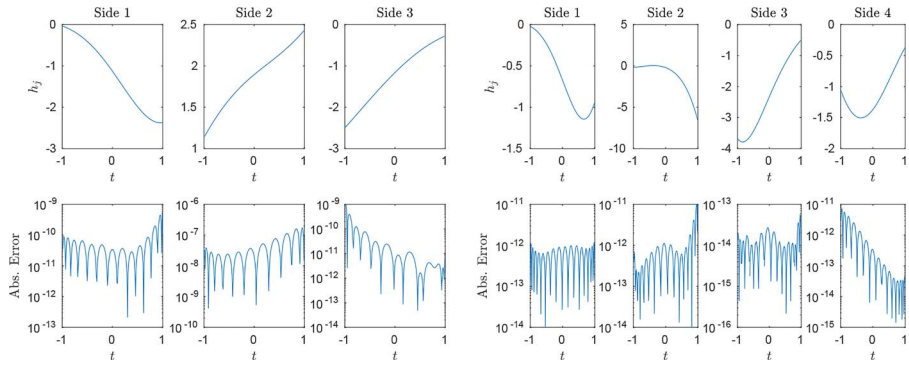

FIG. 12. Results for problem with analytically known solution. Left: $N = 13$ and Ω_1. Right: $N = 17$ and Ω_2.

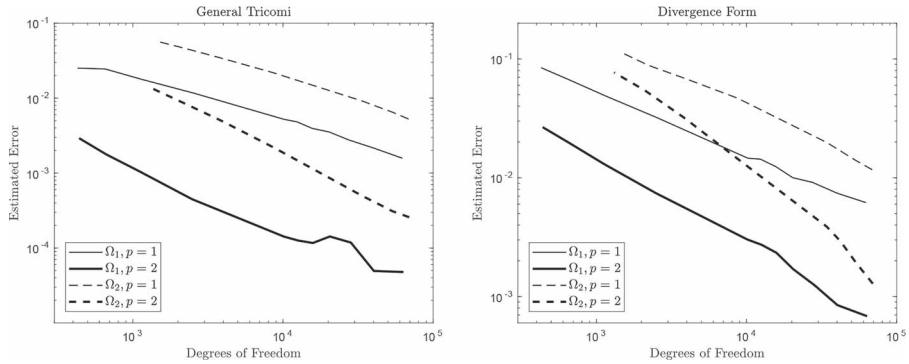

FIG. 13. Convergence rates in presence of corner singularities for FEM, p denotes the polynomial order of the elements. Left: algebraic convergence for Dirichlet problem for the generalized Tricomi equation. Right: algebraic convergence for Dirichlet problem for the general divergence problem.

In this case we follow the remarks in Section 4.4 and give boundary conditions in terms of the oblique derivative

$$\hat{\delta}_j n_j \cdot (\alpha \nabla u_j) + \hat{A}_j u_j = g_j \approx \sum_{l=0}^{N-1} a_l^j P_l(t),$$

$$\hat{A}_j n_j \cdot (\alpha \nabla u_j) - \hat{\delta}_j u_j = h_j \approx \sum_{l=0}^{N-1} b_l^j P_l(t).$$

The domains considered are the same as the previous section (shown in Fig. 9), and we select $\epsilon = 3/2$ to ensure ellipticity.

Our first example uses the same parameter choice as before:

$$(\hat{\delta}_1, \hat{\delta}_2, \hat{\delta}_3) = (1, 0, 1), \qquad (\hat{A}_1, \hat{A}_2, \hat{A}_3) = (1/2, 1, 0), \qquad (\Omega_1),$$
$$(\hat{\delta}_1, \hat{\delta}_2, \hat{\delta}_3, \hat{\delta}_4) = (1, 0, 1, 1), \qquad (\hat{A}_1, \hat{A}_2, \hat{A}_3, \hat{A}_4) = (1/2, 1, 0, 1), \qquad (\Omega_2),$$

but employed the analytic solution

$$u(x, y) = (x + 3/2)\cos(y)\exp(-y).$$

We choose $R = 20$ for Ω_1, and $R = 40$ for Ω_2, with $M = 20N$ for both. As before, the method converges exponentially to this solution with results shown in Fig. 12. Finally, we consider the same Dirichlet boundary conditions

$$u(x, y) = \sin(x), \quad (x, y) \in \partial\Omega,$$

as in Section 5.3. Figures 11 and 13 show the expected algebraic convergence for the unified transform and FEM, respectively. Again we have computed the error by comparing to larger N and a more refined FEM solution. The same conclusions can be drawn as before.

6. Conclusion and future work

We have extended the unified transform of solving the generalized Dirichlet-to-Neumann map to PDEs with variable coefficients and to domains with curved edges. The corresponding global relation (2.6) now involves the integral transforms (2.5). While in general, for a given basis expansion of u and its derivatives, we cannot compute (2.5) explicitly, it was found that the use of a Legendre basis still allows for extremely fast and accurate numerical approximations. The key observation is that the integral transforms are simply rescaled Legendre coefficients which can be approximated by a Chebyshev interpolation. Our numerical results support that this is a fast and competitive method that inherits the convergence properties of the Legendre basis—i.e. it is spectrally accurate for sufficiently smooth solutions and converges algebraically in the presence of corner singularities. A major advantage of the method is that it is a boundary-based method which does not need knowledge of the corresponding Green's function. Hence, it is more applicable than boundary integral methods in the setting of variable coefficients.

The results of Section 5.1 also suggest that in some cases it may be advantageous to break up the domain into several coupled subdomains, and numerical experiments suggest that such decompositions are advantageous if there exist internal angles of π or greater. For straight edges and for the Laplace equation, this advantage can be understood as follows: the exponential 'test functions' grow/decay exponentially in certain directions in the complex plane. When using a sufficiently large selection of complex λ-values, located in all directions from the origin, each side of a convex polygon will encounter for many of these λ-values larger test functions than the remaining sides. In other words, the linear system we seek to solve is block diagonally dominated (Hashemzadeh *et al.*, 2015). However, for nonconvex internal angles this breaks down—boundaries in indented regions will always be dominated by effects from other boundary parts, no matter the λ-value. Simple domain decompositions have been explored in the context of the unified transform in Crowdy & Luca (2014), Crowdy (2015b), Colbrook *et al.* (2018) and Luca & Crowdy (2018). The Dirichlet-to-Neumann map has also been used by Martinsson and collaborators for domain decomposition spectral methods (Martinsson, 2013;

Gillman & Martinsson, 2014; Gillman *et al.*, 2015). Future work will aim to see if the results presented here can be applied to such methods. This could also be an effective route to lower both the complexity of the method presented here and the degree N needed to gain accurate results. It is also likely to be effective at dealing with corner singularities via finer decompositions near the corners of the original domain.

There are several other questions that naturally arise from this study. First, given our choice of the family $\{v(x, y; \lambda) : \lambda \in \mathscr{C}\}$, is the set of equations (2.6) sufficient for determining the generalized Dirichlet to Neumann map? For the case of a convex polygon and a constant coefficient elliptic PDE, assuming the problem has a unique solution (e.g. avoiding eigenvalues of the Laplacian in the Helmholtz/modified Helmholtz case), it was proven in Ashton (2012) that this is indeed the case when using the usual family of exponential solutions. Current work seeks to extend this result to solution families analogous to exponential solutions. The choice of collocation points is also related to numerical complexity and conditioning. For the well-studied case of convex polygons and constant coefficients PDEs, good choices lead to well-conditioned block diagonally dominant linear systems, with the majority of the matrix values exponentially small. For many PDEs such a suitable choice of collocation points may also exist, in which case very small matrix values can be set to zero, resulting in a sparse approximate linear system. Taking advantage of such structure may be an effective way to reduce the complexity of the solution step (now solving a sparse linear system) and also the construction of the linear system by reducing the number of integral transforms that need to be computed. Future work will also aim to take advantage of similar structure. For example, in some cases, the presence of symmetry implies that the collocation matrix (and its least squares inverse) has a semiblock circulant form (Colbrook & Fokas, 2018) that reduces the dimensions of the linear system by a factor of n.

Secondly, can the method be extended to PDEs of higher order? Some results concerning the unified transform applied to the biharmonic equation can be found in (Crowdy & Luca, 2014; Dimakos & Fokas, 2015; Luca & Crowdy, 2018), but in general there are few results in this direction. Thirdly, can the implementation of the unified transform be extended to three dimensions or more generally n-dimensions? Some initial progress in this direction can be found in Hitzazis & Fokas (2017) for cylindrical domains where the global relation and integral representation are generalized, and in Ashton (2015a,b) where the Dirichlet problem is studied, and an integral representation that serves as a concrete realization of the fundamental principle of Ehrenpreis is given. Based on this result, a well-posed Galerkin scheme was constructed and studied numerically in Crooks (2015). In the three dimensional case, this involves the integration of the spectral data over a two dimensional infinite region and hence, poses considerable implementational challenges. Moreover, this method is only available for PDEs with constant coefficients, and so far no similar collocation methods have been implemented in three dimensions. Analogous to Section 2, it is straightforward to write down a global relation using the divergence theorem. If the domain boundary consists of a collection of polytopes, then this leads to $(n-1)$-dimensional integral transforms of the chosen basis functions. The key difficulty then becomes choosing a suitable basis and family of solutions so that these transforms can be computed accurately and efficiently. Such a task remains a challenge, but it is expected that the unified transform still retains a considerable advantage, namely, the reduction of an n-dimensional problem to an $(n-1)$-dimensional problem. A collocation approach to the 3D case is work in progress.

The major drawback of the method proposed in this paper is that it may be difficult to construct a one-parameter family of solutions for the adjoint PDE. Nonetheless, once such family of test functions $\{v(x, y; \lambda) : \lambda \in \mathscr{C}\}$ is constructed, the implementation becomes quite simple as discussed in Section 4. For separable PDEs this is not a problem and hence, the numerical version of the unified transform allows one to deal with separable PDEs on nonseparable domains with nonseparable boundary

conditions. Also, the method adopted for the computation of integral transforms becomes difficult for less regular boundaries, test functions and PDE coefficients. This follows from the larger Chebyshev expansion needed to interpolate the functions. Future work will aim at using the method in this less regular setting and developing/implementing methods to compute the integral transforms in these cases.

Clearly, work is needed in order to address the above issues, but we have provided the first major step in extending the unified transform to curvilinear polygons and to PDEs with variable coefficients. In particular, the unified transform provides a boundary-based method for which the integral transforms can easily be computed, even in these more complicated scenarios, with only small-system sizes needed to achieve very accurate results. Our method of implementation still retains the advantages demonstrated in the literature of the previous collocation-based methods for polygons and constant coefficients, namely, spectral convergence for smooth solutions, speed and the fact that the method is very easy to implement.

Acknowledgements

The author would like to thank Arieh Iserles for many engaging and useful discussions during the completion of this project.

Funding

EPSRC (grant EP/L016516/1 for the University of Cambridge Centre for Analysis).

References

Ashton, A. (2012) On the rigourous foundations of the Fokas method for linear elliptic partial differential equations. *Proc. R. Soc. A*, **468**. 1325–1331.

Ashton, A. (2013) The spectral Dirichlet-Neumann map for Laplace's equation in a convex polygon. *SIAM J. Math. Anal.*, **45**, 3575–3591.

Ashton, A. (2015a) Elliptic PDEs with constant coefficients on convex polyhedra via the unified method. *J. Math. Anal. Appl.*, **425**, 160–177.

Ashton, A. (2015b) Laplace's equation on convex polyhedra via the unified method. *Proc. R. Soc. A.*, **471**, 20140884.

Ashton, A. & Crooks, K. (2016) Numerical analysis of Fokas' unified method for linear elliptic PDEs. *Appl. Numer. Math.*, **104**, 120–132.

Ashton, A. & Fokas, A. (2015) Elliptic boundary value problems in convex polygons with low regularity boundary data via the unified method. *Complex. Var. Elliptic.*, **60**, 596–619.

Babuška, I. & Guo, B. (1988) Regularity of the solution of elliptic problems with piecewise analytic data. Part I. Boundary value problems for linear elliptic equation of second order. *SIAM J. Math. Anal.*, **19**, 172–203.

Babuška, I. & Guo, B. (1989) Regularity of the solution of elliptic problems with piecewise analytic data. II: the trace spaces and application to the boundary value problems with nonhomogeneous boundary conditions. *SIAM J. Math. Anal.*, **20**, 763–781.

Beuchler, S. & Schoeberl, J. (2006) New shape functions for triangular p-FEM using integrated Jacobi polynomials. *Numer. Math.*, **103**, 339–366.

Boyd, J. (2001) *Chebyshev and Fourier Spectral Methods*, 2nd ed. Mineola, NY: Dover Publications.

Colbrook, M., Flyer, N. & Fornberg, B. (2018) On the Fokas method for the solution of elliptic problems in both convex and nonconvex polygonal domains. *J. Comput. Phys.*, **374**, 996–1016.

Colbrook, M. & Fokas, A. (2018) Computing eigenvalues and eigenfunctions of the Laplacian for convex polygons. *Appl. Numer. Math.*, **126**, 1–17.

Crooks, K. (2015) Numerical analysis of the Fokas method in two and three dimensions. *Ph.D. Thesis*, University of Cambridge, UK.

Crowdy, D. (2015a) Fourier–Mellin transforms for circular domains. *Comput. Methods Funct. Theory*, **15**, 655–687.

Crowdy, D. (2015b) A transform method for Laplace's equation in multiply connected circular domains. *IMA J. Appl. Math.*, **80**, 1902–1931.

Crowdy, D. & Luca, E. (2014) Solving Wiener-Hopf problems without kernel factorization. *Proc. R. Soc. A*, **470**, 20140304.

Dassios, G. & Fokas, A. (2005) The basic elliptic equations in an equilateral triangle. *Proc. R. Soc. A*, **461**, 2721–2748.

Davis, C. & Fornberg, B. (2014) A spectrally accurate numerical implementation of the Fokas transform method for Helmholtz-type PDEs. *Complex. Var. Elliptic*, **59**, 564–577.

Deaño, A., Huybrechs, D. & Iserles, A. (2018) *Computing Highly Oscillatory Integrals*, vol. 155. Philadelphia, PA: SIAM.

Deconinck, B., Trogdon, T. & Vasan, V. (2014) The method of Fokas for solving linear partial differential equations. *SIAM Rev.*, **56**, 159–186.

Dimakos, M. & Fokas, A. (2015) The Poisson and the biharmonic equations in the interior of a convex polygon. *Stud. Appl. Math.*, **134**, 456–498.

Fokas, A. (1997) A unified transform method for solving linear and certain nonlinear PDEs. *Proc. R. Soc. A*, **453**, 1411–1443.

Fokas, A. (2000) On the integrability of linear and nonlinear partial differential equations. *J. Math. Phys.*, **41**, 4188–4237.

Fokas, A. (2001) Two–dimensional linear partial differential equations in a convex polygon. *Proc. R. Soc. A*, **457**, 371–393.

Fokas, A. (2004) Boundary-value problems for linear PDEs with variable coefficients. *Proc. R. Soc. A*, **460**, 1131–1151.

Fokas, A. (2008) *A Unified Approach to Boundary Value Problems*. Philadelphia, PA: SIAM.

Fokas, A., Flyer, N., Smitheman, S. & Spence, E. (2009) A semi-analytical numerical method for solving evolution and elliptic partial differential equations. *J. Comput. Appl. Math.*, **227**, 59–74.

Fokas, A. & Kalimeris, K. (2014) Eigenvalues for the Laplace operator in the interior of an equilateral triangle. *Comput. Methods Funct. Theory*, **14**, 1–33.

Fokas, A. & Kapaev, A. (2003) On a transform method for the Laplace equation in a polygon. *IMA J. Appl. Math.*, **68**, 355–408.

Fokas, A. & Pelloni, B. (2014) *Unified Transform for Boundary Value Problems: applications and advances*. Philadelphia, PA: SIAM.

Fokas, A.S. & Spence, E.A. (2012) Synthesis, as opposed to separation, of variables. *Siam Rev.*, **54**, 291–324.

Fokas, A. & Sung, L. (2005) Generalized Fourier transforms, their nonlinearization and the imaging of the brain. *Notices Notices Amer. Math. Soc.*, **52**, 1178–1192.

Fornberg, B. & Flyer, N. (2011) A numerical implementation of Fokas boundary integral approach: Laplace's equation on a polygonal domain. *Proc. R. Soc. A*, **467**, 2983–3003.

Fornberg, B. & Flyer, N. (2015) *A Primer on Radial Basis Functions with Applications to the Geosciences*. Philadelphia, PA: SIAM.

Fulton, S., Fokas, A. & Xenophontos, C. (2004) An analytical method for linear elliptic PDEs and its numerical implementation. *J. Comput. Appl. Math.*, **167**, 465–483.

Gillman, A., Barnett, A. & Martinsson, P.-G. (2015) A spectrally accurate direct solution technique for frequency-domain scattering problems with variable media. *BIT*, **55**, 141–170.

Gillman, A. & Martinsson, P.-G. (2014) A direct solver with $O(N)$ complexity for variable coefficient elliptic PDEs discretized via a high-order composite spectral collocation method. *SIAM J. Sci. Comput.*, **36**, A2023–A2046.

Guo, B. & Babuška, I. (1986) The hp version of the finite element method. *Comput. Mech.*, **1**, 21–41.
Hale, N. & Townsend, A. (2014) A fast, simple, and stable Chebyshev–Legendre transform using an asymptotic formula. *SIAM J. Sci. Comput.*, **36**, A148–A167.
Hashemzadeh, P., Fokas, A. & Smitheman, S. (2015) A numerical technique for linear elliptic partial differential equations in polygonal domains. *Proc. R. Soc. A*, **471**.
Hitzazis, I. & Fokas, A. (2017) Linear elliptic PDEs in a cylindrical domain with a polygonal cross-section. *Stud. Appl. Math.*, **139**, 288–321.
Hydon, P. (2000) *Symmetry Methods for Differential Equations: a Beginner's Guide*, vol. 22. Cambridge: Cambridge University Press.
Kleinman, R., Roach, G. & Ström, S. (1984) The null field method and modified Green functions. *Proc. R. Soc. Lond. A*, **394**, 121–136.
Li, Z.-C. & Lu, T.-T. (2000) Singularities and treatments of elliptic boundary value problems. *Math. Comput.Modelling*, **31**, 97–145.
Li, Z.-C., Lu, T.-T., Hu, H.-Y. & Cheng, A. H. (2008) *Trefftz and Collocation Methods*. Southampton: WIT press.
Luca, E. & Crowdy, D. (2018) A transform method for the biharmonic equation in multiply connected circular domains. *IMA J. Appl. Math.,* doi: 10.1093/imamat/hxy030.
Martin, P. (2006) *Multiple Scattering: Interaction of Time-harmonic Waves with N Obstacles.* Cambridge: Cambridge University Press.
Martinsson, P.-G. (2013) A direct solver for variable coefficient elliptic PDEs discretized via a composite spectral collocation method. *J. Comput. Phys.*, **242**, 460–479.
McLean, W. C. H. (2000) *Strongly Elliptic Systems and Boundary Integral Equations*. Cambridge: Cambridge University Press.
Mukhopadhyay, N., Maiti, S. & Kakodkar, A. (2000) A review of SIF evaluation and modelling of singularities in BEM. *Comput. Mech.*, **25**, 358–375.
Oliveri, F. (2010) Lie symmetries of differential equations: classical results and recent contributions. *Symmetry*, **2**, 658–706.
Olver, S. (2007) Numerical approximation of vector-valued highly oscillatory integrals. *BIT*, **47**, 637–655.
Saridakis, Y., Sifalakis, A. & Papadopoulou, E. (2012) Efficient numerical solution of the generalized Dirichlet–Neumann map for linear elliptic PDEs in regular polygon domains. *J. Comput. Appl. Math.*, **236**, 2515–2528.
Sifalakis, A., Papadopoulou, E. & Saridakis, Y. (2007) Numerical study of iterative methods for the solution of the Dirichlet–Neumann map for linear elliptic PDEs on regular polygon domains. *Int. J. Appl. Math. Comput. Sci.*, **4**, 173–178.
Sifalakis, A., Fokas, A., Fulton, S. & Saridakis, Y. (2008) The generalized Dirichlet–Neumann map for linear elliptic PDEs and its numerical implementation. *J. Comput. Appl. Math.*, **219**, 9–34.
Sifalakis, A., Fulton, S., Papadopoulou, E. & Saridakis, Y. (2009) Direct and iterative solution of the generalized Dirichlet–Neumann map for elliptic PDEs on square domains. *J. Comput. Appl. Math.*, **227**, 171–184.
Smitheman, S., Spence, E. & Fokas, A. (2010) A spectral collocation method for the Laplace and modified Helmholtz equations in a convex polygon. *IMA J. Numer. Anal.*, **30**, 1184–1205.
Spence, E. (2011) Boundary value problems for linear elliptic PDEs. *Ph.D. Thesis*, University of Cambridge, UK.
Spence, E. (2014) When all else fails, integrate by parts: an overview of new and old variational formulations for linear elliptic PDEs. *Unified Transform Method for Boundary Value Problems: Applications and Advances* A. Fokas, B. Pelloni (eds). Philadelphia: SIAM, pp. 93–159.
Spence, E. & Fokas, A. (2010a) A new transform method I: domain-dependent fundamental solutions and integral representations. *Proc. R. Soc. A*, **466**, 2259–2281.
Spence, E. & Fokas, A. (2010b) A new transform method II: the global relation and boundary-value problems in polar coordinates. *Proc. R. Soc. A*, **466**, 2283–2307.
Stakgold, I. (2000) *Boundary Value Problems of Mathematical Physics: 2-Volume Set*, vol. 29. Philadelphia, PA: SIAM.

Symm, G. (1973) *Treatment of singularities in the solution of Laplace's equation by an integral equation method*. *Report NAC 31*. National Physical Laboratory, Division of Numerical Analysis and Computing.

Townsend, A., Webb, M. & Olver, S. (2018) Fast polynomial transforms based on Toeplitz and Hankel matrices. *Math. Comp.*, **87**, 1913–1934.

Treharne, P. & Fokas, A. (2007) Initial-boundary value problems for linear PDEs with variable coefficients. *Math. Proc. Camb. Philos. Soc.*, **143**, 221–242.

Zhu, Y. & Cangellaris, A. (2006) *Multigrid Finite Element Methods for Electromagnetic Field Modeling*, vol. 28. Hoboken, NJ: John Wiley & Sons.

Appendix. Effect of the Choice of R

Figure A1 shows the errors and condition numbers for the BVPs in Section 5.1 as functions of R for $N = 10$, $M = 200$ and $x_0 = -3/2$. In general, increasing M reduces the condition number, but for a fixed M there is a wide range of values of R which yield similar results. The degradation of accuracy for $R > 40$ is not due to errors in approximating the integrals numerically—the same effect occurs for the strict polygonal case where we have analytic forms of the integrals.

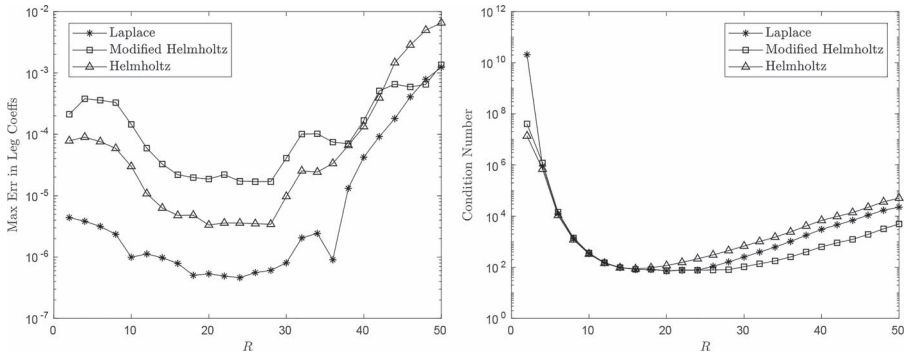

Fig. A1. Left: maximum errors in Legendre coefficients for the unknown boundary values as functions of R. Right: condition numbers of the systems as functions of R.